THE EUROPEAN
PHYSICAL JOURNAL C

DPS mechanism for associated $c\bar{c}b\bar{b}$ production in AA UPCs

Edgar Huayra[1,a], **Emmanuel G. de Oliveira**[1,b], **Roman Pasechnik**[1,2,c]

[1] Departamento de Física, CFM, Universidade Federal de Santa Catarina, C.P. 476, Florianópolis, SC CEP 88.040-900, Brazil
[2] Department of Astronomy and Theoretical Physics, Lund University, 223 62 Lund, Sweden

Abstract We discuss the associated $c\bar{c}$ and $b\bar{b}$ quark pairs production in the double-parton scattering (DPS) process in ultraperipheral (UPCs) AA collisions. We derive an analogue of the inclusive DPS pocket formula and the photon-energy dependent effective cross section considering an overlap between the hard SPS scatterings. We provide numerical predictions for the DPS cross sections for the $c\bar{c}b\bar{b}$ production process at the typical energies of AA UPCs at the LHC and FCC colliders and also characterize the A dependence of the total UPC DPS cross section.

1 Introduction

The double- or, generally, multi-parton interaction (MPI) processes become increasingly important in hadron-hadron and especially nucleus-nucleus collisions at high energies. In particular, the ratio of probabilities of the double-parton scattering (DPS) to single-parton scattering (SPS) grows in energy [1–3] and cannot be neglected already at the LHC. In connection to the LHC measurements, a significant amount of work, both experimental and theoretical, has been done in analysis of MPI contributions to hadroproduction reactions with many different final states, see e.g. Refs. [4–12] and references therein. Most common examples with a significant DPS effect include meson pairs [10], four identified jets [11] or leptons [12] etc. In fact, the MPIs are naturally accounted for in most commonly used event generators [3,13].

From theoretical viewpoint, the DPS processes are connected to yet poorly known double-parton distribution functions (dPDFs) which are of a predominantly non-perturbative QCD origin and remain highly uncertain (for a detailed review on the theoretical basis of dPDFs, see e.g. Ref. [14] and references therein). These objects represent number den-

sities of correlated pairs of two colored partons (quark and gluons) in the proton or a nucleus carrying longitudinal momentum fractions x_1 and x_2 that are found at a particular transverse relative separation **b** between subsequent two hard scatterings [15]. While the first-principle calculations of dPDFs with non-perturbative parton correlations are yet not feasible theoretically, several models attempting to capture the most relevant dPDFs properties are being advised in the literature, see e.g. Refs. [8,9,16–18].

Relevant phenomenological information about dynamics of dPDFs is contained in a measurable quantity known as effective cross section, σ_{eff} that is being extensively studied in various particle production channels [11,12,19–25]). Among the final states, such processes as the associated double open heavy flavor production and heavy flavor production in association with jets are typically considered as a powerful toolkit for probing the DPS dynamics, see its earlier studies in non-peripheral collisions in Refs. [10,21,26–29]

In our earlier analysis of Ref. [30] we performed a first study of double open heavy flavor production, specifically, in high-energy ultraperipheral collisions (UPCs) focusing on the $c\bar{c}b\bar{b}$ final states produced off the proton target. An enhanced double-photon flux coming from the incident nucleon has been considered as a probe for the double-gluon density in the proton. Among the advantages of using the pA and AA UPCs compared to more standard central pp collisions for probing the MPIs are a relatively low QCD background provided by tagging on the final-state nucleus and a strongly enhanced quasi-real Weizsäcker–Williams (WW) photon flux [31,32] in the incident nucleus, with a rather broad photon spectrum.

As usual, the effective cross section in this case corresponds to an effective transverse overlap area between hard single-parton scatterings and is conventionally defined as a ratio between the product of SPS cross sections, $\sigma_{\text{SPS}}^{c\bar{c}}$ and $\sigma_{\text{SPS}}^{b\bar{b}}$, over the production cross section going via the DPS

[a] e-mail: yuberth022@gmail.com

[b] e-mail: emmanuel.de.oliveira@ufsc.br

[c] e-mail: Roman.Pasechnik@thep.lu.se (corresponding author)

mechanism, $\sigma_{\mathrm{DPS}}^{c\bar{c}b\bar{b}}$, such that

$$\sigma_{\mathrm{eff}} = \frac{\sigma_{\mathrm{SPS}}^{c\bar{c}}\sigma_{\mathrm{SPS}}^{b\bar{b}}}{\sigma_{\mathrm{DPS}}^{c\bar{c}b\bar{b}}}, \tag{1}$$

Under an approximation when the effective cross section is not dependent on the kinematics of the underlined process and is considered as a constant geometrical factor, Eq. (1) is known as the "pocket formula". Switching from the two-gluon initial state to the two-photon one coming from the initial nucleus, it was shown in Ref. [30] that the effective cross section becomes significantly larger than for four-parton initial state and amounts to, roughly, a few dozens of barns. Besides, due to a wide-spread photon distribution, σ_{eff} strongly depends on the photon longitudinal momentum fraction such that a naive multiplication of SPS cross sections in Eq. (1) does not apply any longer and one has to perform a convolution in the photon momentum fraction.

In the current study, we consider the same type of process as an efficient probe for the double-gluon density in the target nucleus at small-x and compute the corresponding DPS contribution to the observables at different energies. For this purpose, we extend our previous study [30] to heavy-ion AA UPCs with the focus of probing the gluon dPDFs in the $A+A \rightarrow A+(c\bar{c}b\bar{b})+X$ reaction by means of double-photon exchange with another nucleus at large impact parameters. Particularly, this process represents a novel and clean way of probing small-x gluon dPDFs in a nucleus competitive to more standard processes in central collisions.

The paper is organised as follows. In Sect. 2, we discuss the basics of the SPS contribution to the inclusive differential $c\bar{c}b\bar{b}$ production cross section setting up all the necessary ingredients for the DPS analysis. In Sect. 3, we describe two distinct contributions to the DPS mechanism of $c\bar{c}b\bar{b}$ production in AA UPCs coming from uncorrelated (on two different nucleons) and correlated (on a single nucleon) SPS processes. Here, we also derive the generalised UPC pocket formula accounting for both contributions and the corresponding effective cross section. In Sect. 4, we present numerical results for the effective cross section and for the differential DPS cross sections for double heavy-quark pair production in AA UPCs at typical LHC and FCC energies. Finally, basic conclusions are made in Sect. 5.

2 Single-parton scattering

The kinematics of the considered $A + A \rightarrow A + (c\bar{c}b\bar{b}) + X$ process and details of calculations are rather similar to those in the $A + p \rightarrow A + (c\bar{c}b\bar{b}) + X$ previously discussed in Ref. [30]. So, here we only briefly discuss the most crucial elements of the formalism particularly relevant for the direct $c\bar{c}b\bar{b}$ production reaction in AA UPCs.

To start with let us define the photon and gluon longitudinal momentum fractions as follows

$$\xi_i = \frac{m_{i,\perp}}{\sqrt{s}}(e^{y_{Q_i}} + e^{y_{\bar{Q}_i}}), \quad x_i = \frac{m_{i,\perp}}{\sqrt{s}}(e^{-y_{Q_i}} + e^{-y_{\bar{Q}_i}}),$$
$$m_{i,\perp}^2 = m_{Q_i}^2 + p_{i,\perp}^2, \tag{2}$$

Here, $i = 1, 2$ correspond to separate hard SPS photon-gluon fusion $\gamma g \rightarrow c\bar{c}$ and $\gamma g \rightarrow b\bar{b}$ subprocesses, respectively, such that $Q_{1,2} \equiv c, b$, while $m_{i,\perp}$ and y_{Q_i} ($y_{\bar{Q}_i}$) are the (anti)quark transverse mass and rapidity, respectively.

The cross section for $Q\bar{Q}$-pair production in the SPS AA UPCs can be represented as a convolution of parton-level $\gamma + g \rightarrow Q\bar{Q}$ subprocess cross section off a given nucleon in the nucleus target with the spatial nucleon density in the nucleus given by the so-called nuclear thickness function $\rho(\vec{b}_p)$, as well as the gluon distribution in the nucleon, G_g^A, in the following form[1]

$$\frac{d^2\sigma_{AA\rightarrow XA+Q\bar{Q}}}{dy_Q dy_{\bar{Q}}} = \int d^2\vec{b}d^2\vec{b}_\gamma d^2\vec{b}_p d^2\vec{b}_g d\xi dx \Theta(b - 2R_A)$$
$$\times \delta^{(2)}(\vec{b} + \vec{b}_p + \vec{b}_g - \vec{b}_\gamma)$$
$$\times N_\gamma(\xi, \vec{b}_\gamma)G_g^A(x, \vec{b}_g)\rho(\vec{b}_p)\frac{d^2\hat{\sigma}_{\gamma g\rightarrow Q\bar{Q}}}{dy_Q dy_{\bar{Q}}}, \tag{3}$$

$$\frac{d^2\hat{\sigma}_{\gamma g\rightarrow Q\bar{Q}}}{dy_Q dy_{\bar{Q}}} = \int d\hat{t}\frac{d\hat{\sigma}_{\gamma g\rightarrow Q\bar{Q}}}{d\hat{t}}\delta\left(y_Q - \frac{1}{2}\ln\left(\frac{\xi}{x}\frac{\hat{u}}{\hat{t}}\right)\right)$$
$$\times \delta\left(y_{\bar{Q}} - \frac{1}{2}\ln\left(\frac{\xi}{x}\frac{\hat{t}}{\hat{u}}\right)\right), \tag{4}$$

$$\hat{t} = (p_Q - p_\gamma)^2 - m_Q^2 = -\sqrt{\hat{s}}\left(\frac{\sqrt{\hat{s}}}{2} - \sqrt{\frac{\hat{s}}{4} - m_Q^2 - p_\perp^2}\right), \tag{5}$$

in terms of the $Q\bar{Q}$ invariant mass squared $\hat{s}$, nucleus radius R_A, (quasi-real) WW single-photon flux in the nucleus N_γ,

$$\frac{d^3N_\gamma(\xi, \vec{b})}{d\xi d^2\vec{b}} = \frac{\sqrt{s}}{2}\frac{Z^2\alpha k^2}{\pi^2\omega b^2}\left[K_1^2(k) + \frac{1}{\gamma^2}K_0^2(k)\right],$$
$$k = \frac{b\omega}{\gamma}, \quad \xi = \frac{2\omega}{\sqrt{s}}, \tag{6}$$

and the nucleon single-gluon G_g^A distribution [33],

$$G_g^A(x, \vec{b}_g) = A g_A(x) f_g(\vec{b}_g),$$
$$f_g(\vec{b}) = \frac{\Lambda^2}{2\pi}\frac{\Lambda b}{2}K_1(\Lambda b), \quad \int d^2\vec{b} f_g(\vec{b}) = 1. \tag{7}$$

Above, A and Z are the atomic mass and the electric charge of the nucleus, respectively, $K_{0,1}$ are the modified Bessel functions of the second kind, α is the fine structure constant, ω is the exchanged photon energy, $\gamma = \sqrt{s}/2m_p$ is the

---

[1] We assume for simplicity that the scattered nuclei are the same.

Lorentz factor defined in terms of the total center-of-mass (c.m.) energy per nucleon squared, s, and the proton mass $m_p = 0.938$ GeV. The distribution $g_A(x)$ is the collinear gluon density in the nucleon in a given nucleus A for which the EPPS16nlo [34] parameterisation has been used (with the factorisation scale $\mu_F = \hat{s}$), $f_g(\vec{b})$ is the normalised spatial gluon density in a nucleon inside the nucleus, the scale parameter $\Lambda \approx 1.5$ GeV. In what follows, the thickness function $\rho(\vec{b}_p)$ has been adopted in the Woods-Saxon parameterisation [35],

$$\rho(\vec{b}_p) = \rho_0 \int dz \frac{1}{1 + \exp\left(\frac{\sqrt{\vec{b}_p^2 + z^2} - R_A}{\delta}\right)},$$

$$\int d^2\vec{b}_p \, \rho(\vec{b}_p) = 1, \qquad (8)$$

where ρ_0 is an overall normalisation, and $\delta = 0.459$ fm with $R_A = [1.1 A^{1/3} - 0.65 A^{-1/3}]$ fm to $4 \leq A \leq 208$. Provided that the spatial gluon distribution in the nucleon is much narrower than that of the photon, the SPS cross section (5) can be conveniently rewritten in terms of the collinear gluon density as follows

$$\frac{d^2\sigma_{AA \to A(Q\bar{Q})X}}{dy_Q dy_{\bar{Q}}} = \int d\xi \int dx \, \overline{N}_\gamma(\xi) \, A g_A(x) \frac{d^2\hat{\sigma}_{\gamma g \to Q\bar{Q}}}{dy_Q dy_{\bar{Q}}}$$

$$\times \int d^2\vec{b} \, \Theta(b - 2R_A) T_{g\gamma}(\xi, \vec{b}). \qquad (9)$$

Here, the number distribution of interacting photons averaged over their transverse positions outside the nucleus target reads

$$\overline{N}_\gamma(\xi) = \int d^2 b \, \Theta(b - R_A) N_\gamma(\xi, \vec{b}), \qquad (10)$$

and the overlap function

$$T_{g\gamma}(\xi, \vec{b}) = \frac{1}{\overline{N}_\gamma(\xi)} \int d^2\vec{b}_p \int d^2\vec{b}_\gamma \, \Theta(b_\gamma - R_A) N_\gamma(\xi, \vec{b}_\gamma)$$

$$\times f_g(\vec{b}_\gamma - \vec{b}_p - \vec{b}) \, \rho(\vec{b}_p), \qquad (11)$$

provides an information about the impact parameter dependence of the matrix element squared.

3 Double-parton scattering

In variance to the proton target case studied earlier in Ref. [30] and generalizing the pp approach of the Ref. [15], for the nucleus target there are two distinct contributions to the DPS UPC cross section

$$\sigma_{AA}^{DPS} = \sigma_I^{DPS} + \sigma_{II}^{DPS}. \qquad (12)$$

The first contribution here corresponds to the situation when two SPS gluons are taken from two different nucleons in the nucleus as illustrated in Fig. 1(left), while the second contribution emerges when the two gluons come from a single nucleon as in Fig. 1(right). In what follows, we neglect any differences between proton and neutron in the nucleus target which is an approximation suitable in the high-energy regime.

3.1 Scattering off different nucleons

The DPS cross section for the first case in Fig. 1(left) can be represented as a convolution of the parton-level SPS cross sections [30],

$$\frac{d^4\sigma_I^{DPS}}{dy_c dy_{\bar{c}} dy_b dy_{\bar{b}}}$$

$$= \int d^2 b \, \Theta(b - 2R_A) \int d^2\vec{b}_{\gamma,1} \, \Theta(b_{\gamma,1} - R_A)$$

$$\times \int d^2\vec{b}_{\gamma,2} \, \Theta(b_{\gamma,2} - R_A)$$

$$\times \int d\xi_1 d\xi_2 dx_1 dx_2 N_{\gamma\gamma}(\xi_1, \vec{b}_{\gamma,1}; \xi_2, \vec{b}_{\gamma,2})$$

$$\times \mathcal{G}_{gg}^A(x_1, \vec{b}_{\gamma,1} - \vec{b}; x_2, \vec{b}_{\gamma,2} - \vec{b}) \frac{d^2\hat{\sigma}_{\gamma g \to c\bar{c}}}{dy_c dy_{\bar{c}}} \frac{d^2\hat{\sigma}_{\gamma g \to b\bar{b}}}{dy_b dy_{\bar{b}}},$$

where $N_{\gamma\gamma}$ and $\mathcal{G}_{gg}^A$ are the nuclear di-photon and di-gluon densities, and the impact parameters from the center of the nucleus for each of the two gluons are $\vec{b}_{g,i} + \vec{b}_{p,i} = \vec{b}_{\gamma,i} - \vec{b}$. Following Ref. [30], we neglect possible correlations between photon and gluon exchanges that belong to separate SPS subprocesses. Such an approximation implies factorisation of di-photon $N_{\gamma\gamma}^A$ and di-gluon $\mathcal{G}_{gg}^A$ densities justified in the high-energy regime $\xi_{1,2}, x_{1,2} \ll 1$ [4,9,16,36,37],

$$N_{\gamma\gamma}(\xi_1, \vec{b}_{\gamma,1}; \xi_2, \vec{b}_{\gamma,2}) = N_\gamma(\xi_1, \vec{b}_{\gamma,1}) N_\gamma(\xi_2, \vec{b}_{\gamma,2}),$$
$$\mathcal{G}_{gg}^A(x_1, \vec{b}_{\gamma,1} - \vec{b}; x_2, \vec{b}_{\gamma,2} - \vec{b}) = \mathcal{G}_g^A(x_1, \vec{b}_{\gamma,1} - \vec{b}) \mathcal{G}_g^A(x_2, \vec{b}_{\gamma,2} - \vec{b})$$
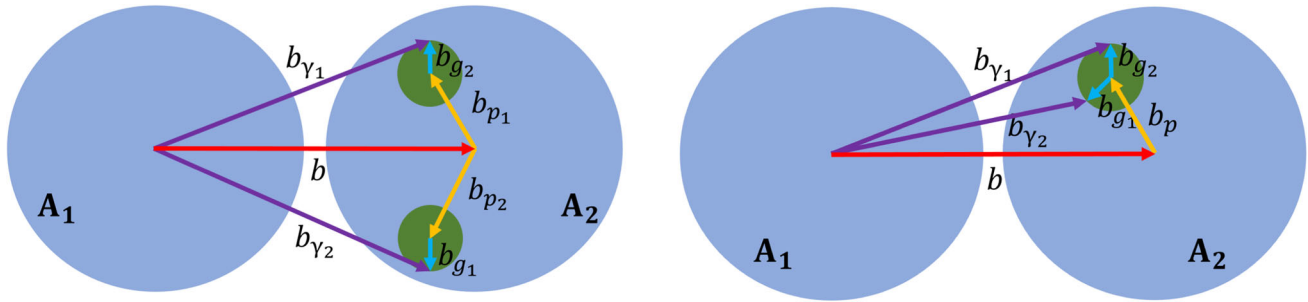
$$(13)$$

where

$$\mathcal{G}_g^A(x, \vec{b}_\gamma - \vec{b})$$

$$= \int d^2 b_p \, G_g^A(x, \vec{b}_\gamma - \vec{b} - \vec{b}_p) \rho(\vec{b}_p). \qquad (14)$$

This equation, together with Eqs. (7) and (11), enables one to represent the effective cross section that corresponds to the first contribution in Fig. 1(left) as follows (c.f. Ref. [30])

$$\sigma_{eff,I}^{-1}(\xi_1, \xi_2) \equiv \int d^2 b \, \Theta(b - 2R_A) T_{g\gamma}(\xi_1, b) T_{g\gamma}(\xi_2, b),$$

$$(15)$$

such that the nuclear density function enters via $T_{g\gamma}(\xi_1, b)$, as defined in Eq. (11). In the UPC kinematics, as usual, the dis-

Fig. 1 Two distinct contributions to the DPS cross section in AA UPCs. On the left, the two photons from the projectile interact with two gluons originating from different nucleons; its contribution to the DPS cross section is proportional to $A - 1$ and will be the dominant one for large A. On the right, the photons interact with gluons from the same nucleon

tance between the nuclear centres $\vec{b}$ (i.e. the collision impact parameter) is integrated out over the region of large $b > 2R_A$.

3.2 Scattering off a single nucleon

Since both gluons interacting with two projectile photons in the DPS mechanism as depicted in Fig. 1(right) belong to the same nucleon, there is no factorisation between the amplitudes for the corresponding SPS processes. In this case, the inverse effective cross section can be obtained in analogy to Eq. (15) as an integral over the impact parameter of the collision $\vec{b}$ outside both the nuclei, i.e.

$$\sigma_{\text{eff,II}}^{-1}(\xi_1, \xi_2) \equiv \int d^2b \, \Theta(b - 2R_A)$$
$$\times \int d^2b_p \, \rho(\vec{b}_p) \, \tau_{g\gamma}(\xi_1, \vec{b}_p + \vec{b}) \tau_{g\gamma}(\xi_2, \vec{b}_p + \vec{b}), \quad (16)$$

where $\tau_{g\gamma}$ is the differential inverse overlap function defined as follows

$$\tau_{g\gamma}(\xi, \vec{b}_p + \vec{b}) = \frac{1}{\overline{N}_\gamma(\xi)} \int d^2b_\gamma \, \Theta(b_\gamma - R_A) N_\gamma(\xi, \vec{b}_\gamma)$$
$$\times f_g(\vec{b}_\gamma - \vec{b}_p - \vec{b}) \quad (17)$$

Indeed, this function depends on the momentum fractions of the interacting photons $\xi_{1,2}$. Due to an additional integral over the nucleon impact parameter $\vec{b}_p$ w.r.t. to the center of the nucleus, such dependencies do not factorise, being an important example of correlations in the two-gluon distribution.

3.3 Pocket formula

In order to combine the two contributions discussed above to the resulting DPS $c\bar{c}b\bar{b}$ production cross section, one has to make sure that the same nucleon does not interact twice when considering the first process in Fig. 1(left). Besides, it is important to take into account that all the nucleons in the target nucleus participate in the interaction corresponding to

the second process in Fig. 1(right). Requiring that these two conditions are satisfied simultaneously, we can construct the generalised pocket formula for the DPS cross section

$$\frac{d^2\sigma_{AA \to A(c\bar{c}b\bar{b})X}^{\text{DPS}}}{dy_c dy_b}$$
$$= \int d\xi_1 \int d\xi_2 \frac{1}{\sigma_{\text{eff}}^{AA}(\xi_1, \xi_2)} \frac{d^2\sigma_{AA \to A(c\bar{c})X}^{\text{SPS}}}{dy_c d\xi_1} \frac{d^2\sigma_{AA \to A(b\bar{b})X}^{\text{SPS}}}{dy_b d\xi_2}.$$
$$(18)$$

Here, the differential SPS cross sections $AA \to A(Q\bar{Q})X$ for $Q = c, b$ can be found starting from Eq. (5), and effective cross section is composed of two contributions from each of the DPS processes discussed above

$$\frac{1}{\sigma_{\text{eff}}^{AA}(\xi_1, \xi_2)} = \frac{w_1}{\sigma_{\text{eff,I}}(\xi_1, \xi_2)} + \frac{w_2}{\sigma_{\text{eff,II}}(\xi_1, \xi_2)}, \quad (19)$$

where $\sigma_{\text{eff,I}}$ and $\sigma_{\text{eff,II}}$ are the effective cross sections for each process defined in Eqs. (15) and (16), respectively, and the corresponding weight factors read

$$w_1 = \frac{A-1}{A}, \qquad w_2 = \frac{1}{A} \quad (20)$$

in terms of the atomic mass A. Let us now turn to numerical results.

4 Numerical results

In the analysis of the DPS cross section of double heavy-flavor $c\bar{c}b\bar{b}$ production in AA UPCs, we present the results for lead-lead nuclei collisions firstly, with $A = 208$. The lead nucleus radius is taken to be $R_A = 5.5$ fm, and the charm and bottom quark masses are $m_c = 1.4$ GeV and $m_b = 4.75$ GeV, respectively. In the case of such a heavy nucleus, more than 99% of the contribution to this process is due to the Part-I contribution that probes gluons at different nucleons. Even for a lighter target, such as the one in a lead–carbon
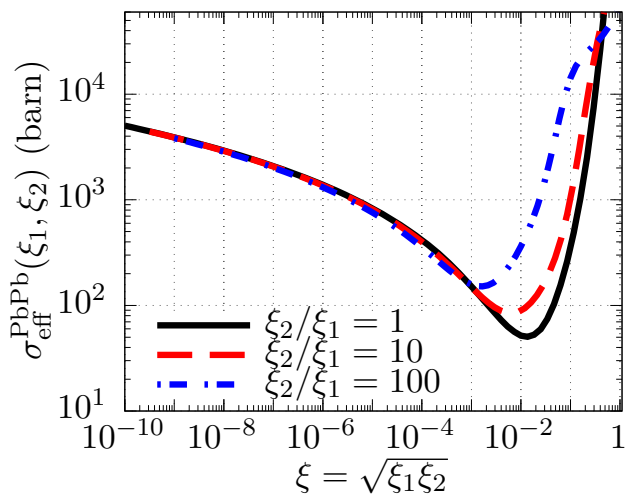
Fig. 2 The DPS effective cross section of $c\bar{c}b\bar{b}$ production in PbPb UPCs as a function of $\xi \equiv \sqrt{\xi_1 \xi_2}$

collision, the part-I contribution to the cross-section is still above 90%.

The behavior of effective cross section for lead-lead UPCs constructed above in Eq. (19) is shown in Fig. 2 as a function of the geometric mean of the two photon momentum fractions, $\xi = \sqrt{\xi_1 \xi_2}$. This plots provides a clear idea of a typical photon energy but does not represent the typical number densities of photons outside the given nucleus since this information has been factorised and absorbed into $\overline{N}_\gamma(\xi)$ function.

Similarly to what has been observed earlier in pA UPCs in Ref. [30], in the case-I depicted in Fig. 1(left) the main contribution to the effective cross section emerges due to configurations when each of the two incoming photons "meet" the gluons inside each of the interacting nucleons. Likewise, in the case-II shown Fig. 1(right) the effective cross section is dominated by the configurations where both photons interact

with gluons inside the same nucleon. Indeed, considering the symmetric configuration $\xi_1 = \xi_2$ as a representative example, for small ξ the photons rarely overlap and σ_{eff}^{AA} is large, while for large ξ the photons are accumulated in a shell at the projectile nucleus periphery.

Clearly, when at some critical ξ value the width of such a shell becomes narrower than the nucleon radius, the effective cross section grows again. Therefore, the photons do overlap for large ξ, but not inside the target nucleus, where most of the target gluons are located. Interestingly, in the AA UPCs σ_{eff}^{AA} develops a minimum at several times smaller than in the pA UPCs case, i.e. at $\xi \approx 0.013$. This is due to the fact that the positions of "active" nucleons are widely distributed in the target nucleus according to the nuclear density. In the minimum of σ_{eff}^{AA}, approximately half of the photons outside the projectile nucleus have $b_\gamma \lesssim 2R_{\text{Pb}}$, i.e. located at the distance approximately equal to or smaller than the radius of the second, target nucleus.

Note, in the considered analysis, to a good approximation, no dependence of σ_{eff}^{AA} on collision energy or the factorisation scale is accounted for. In the considered formulation such an effect is subleading as may potentially only come from an effect of broadening of the impact parameter distribution of the gluon density at high energies. As long as the gluon distribution is well localized compared to the photon distribution, it is not an important factor as the many experiments that measure $\sigma_{\text{eff}} \simeq 15$ mb in pp collisions confirm. We leave this potentially interesting aspect for further, more quantitative, investigations elsewhere.

In Fig. 3, we present the DPS $c\bar{c}b\bar{b}$ production cross sections at two distinct energies, $\sqrt{s} = 5.02$ TeV at the LHC and 39.4 TeV, corresponding to the planned measurements at the Future Circular Collider (or FCC). Here, the cross section is taken to be differential in y_c (left panel) and y_b (right panel), while integrated in $y_{\bar{c}}$ and $y_{\bar{b}}$, respectively. As we know from
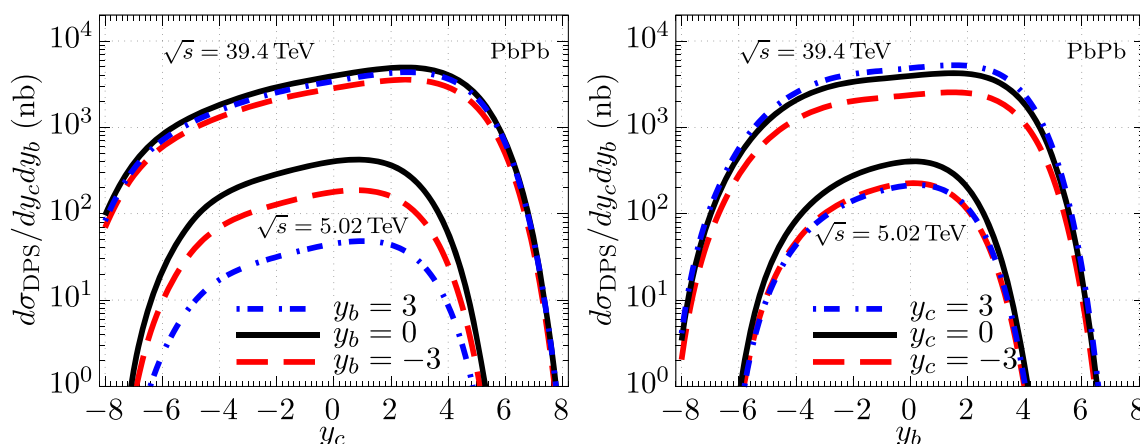
Fig. 3 The DPS $c\bar{c}b\bar{b}$ production cross section in AA UPCs at typical LHC ($\sqrt{s} = 5.02$ TeV) and FCC ($\sqrt{s} = 39.4$ TeV) energies as a function of c-quark rapidity at fixed b-quark rapidity (left panel) and as a function of b-quark rapidity at fixed c-quark rapidity (right panel)
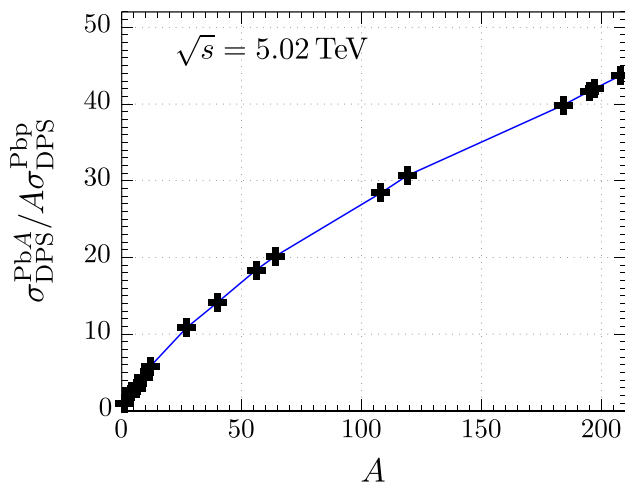
Fig. 4 The atomic mass dependence of the total DPS cross section in the AA UPCs at $\sqrt{s} = 5.02$ TeV relative to that in pA UPCs. Here, the projectile lead nucleus is adopted while A of the target nucleus is a variable quantity corresponding to the parameterisations provided by the EPPS16 nuclear PDFs

earlier studies in Ref. [30], the considered DPS cross sections can not be obtained by a simple rescaling of the corresponding SPS cross sections that makes our result nontrivial and important. Confirming this interpretation, the shape of the cross section as a function of the first quark rapidity changes as we vary the second quark rapidity. Additionally, since the behavior of the gluon and the photon distributions are different with x and ξ, respectively, we observe that the cross section at central rapidities grows with quark rapidity.

Finally, in Fig. 4 we present our prediction for the A dependence of the total DPS cross section in the $Pb + A$ UPCs at $\sqrt{s} = 5.02$ TeV relative to that in $Pb + p$ UPCs. Here, Pb denotes the projectile nucleus as a source of the di-photon flux, while A corresponds to the target nucleus and is varied in our analysis. Similarly to the definition of the nuclear modification factor, this ratio is taken to be normalised to A. Table 1 represents the values for the integrated DPS cross section (in nb) divided by target atomic number A for different values of A. We observe an approximately linear enhancement of this ratio in A at large A, in overall consistency with simulations of the inclusive DPS cross section off proton versus nuclear targets found recently in Ref. [13]. However, the growth in UPCs is steeper, since here the target gluons are probed by projectile photons that are more spread than projectile gluons and thus are more dependent on the size of target.

5 Conclusions

In this work, we present the first analysis of the double heavy-quark pair $c\bar{c}b\bar{b}$ production in AA UPCs as a further development of our previous work [30] studying such process in pA UPCs.

We extended to UPCs the idea, already used in studies of inclusive production, of splitting the cross section into two parts: the first in which the photons interact with different nucleons in the nucleus (and therefore the two target gluons are not correlated) and the second in which the photons interact with two (correlated) gluons from the same nucleon. The latter is an important effect, and such correlations in the two-gluon distribution is a hot topic in the inclusive production off the proton target.

As a result, for the first time we have computed the effective cross section in AA UPCs, i.e., two photon–two gluon double-parton scattering (DPS). As the photon impact parameter distribution depends on the photon energy in a non negligible way, this quantity does exhibit a certain variation on longitudinal momentum fractions $\xi_{1,2}$ for each incident photon. We observe an absolute minimum in the effective UPC cross section when $\xi_1 = \xi_2 \approx 0.013$ in the case of lead nucleus, when the photons are mostly localised in a shell around the projectile nucleus of width roughly of the size of the target nucleus.

We made predictions for the PbPb DPS UPC cross section at two different energies (LHC and FCC) as a functions of both quark rapidities y_c and y_b. The shape of the cross section as a function of the first quark rapidity changes as we vary the second quark rapidity, contrary to the case in which the effective cross section is just a constant. If the data confirm this behaviour, this would be conclusive signature of the pocket formula not having a constant σ_{eff}^{AA} as indicated by our calculations.

Taking the lead nucleus as the projectile and varying the target nucleus A, we see a steep rise of the UPC DPS production cross section. This is a stronger rise than the one found in the inclusive AA case. In short, this means that multiple parton interactions in UPCs happen much more often that in the inclusive case. For instance, when comparing the lead and proton targets, we obtain a factor of about 44 increase. This factor gives a motivation to perform such measurements at a larger integrated luminosity in the LHC Run 3 and, eventually, at the HL-LHC.

Table 1 Integrated DPS cross section (in nb) divided by target atomic number A for different values of A

A	1	4	6	9	12	27	40	56	64	108	119	184	195	197	208
$\sigma_{\text{DPS}}^{PbA}/A$	1.36	3.42	3.93	5.93	7.91	13.70	19.25	24.95	27.38	38.59	41.65	54.14	56.60	57.05	59.40

Data Availability Statement This manuscript has no associated data or the data will not be deposited. [Authors' comment: This is a theoretical work which does not contain any data to be deposited.].

References

1. N. Paver, D. Treleani, Nuovo Cim. A **70**, 215 (1982)
2. M. Mekhfi, Phys. Rev. D **32**, 2371 (1985)
3. T. Sjostrand, M. van Zijl, Phys. Rev. D **36**, 2019 (1987)
4. J.R. Gaunt, W.J. Stirling, JHEP **03**, 005 (2010). arXiv:0910.4347
5. M. Diehl, D. Ostermeier, A. Schafer, JHEP. **03**, 089 (2012), [Erratum: JHEP03,001(2016)]. arXiv:1111.0910
6. A.V. Manohar, W.J. Waalewijn, Phys. Rev **D85**, 114009 (2012). arXiv:1202.3794
7. R. Aaij et al. (LHCb), JHEP. **07**, 052 (2016). arXiv:1510.05949
8. B. Blok, M. Strikman, Eur. Phys. J **C76**, 694 (2016). arXiv:1608.00014
9. M. Rinaldi, S. Scopetta, M. Traini, V. Vento, Phys. Lett. **B752**, 40 (2016). arXiv:1506.05742
10. R. Maciula, A. Szczurek, Phys. Rev. **D97**, 094010 (2018). arXiv:1803.01198
11. F. Abe et al., CDF. Phys. Rev. D **47**, 4857 (1993)
12. M. Aaboud et al. (ATLAS), Phys. Lett. **B790**, 595 (2019) [Phys. Lett.790,595(2019)]. arXiv:1811.11094
13. O. Fedkevych, L. Lönnblad (2019). arXiv:1912.08733
14. M. Diehl, J.R. Gaunt, Adv. Ser. Direct. High Energy Phys **29**, 7 (2018). arXiv:1710.04408
15. G. Calucci, D. Treleani, Phys. Rev. D **60**, 054023 (1999). arXiv:hep-ph/9902479
16. H.-M. Chang, A.V. Manohar, W.J. Waalewijn, Phys. Rev. **D87**, 034009 (2013). arXiv:1211.3132
17. M. Rinaldi, S. Scopetta, V. Vento, Phys. Rev. **D87**, 114021 (2013). arXiv:1302.6462
18. M. Rinaldi, S. Scopetta, M. Traini, V. Vento, JHEP **12**, 028 (2014). arXiv:1409.1500
19. T. Åkesson et al., Axial field spectrometer. Z. Phys. C **34**, 163 (1987)
20. J. Alitti et al., UA2. Phys. Lett. B **268**, 145 (1991)
21. R. Aaij et al. (LHCb), JHEP.**06**, 141 (2012), [Addendum: JHEP03,108(2014)]. arXiv:1205.0975
22. V. M. Abazov et al. (D0), Phys. Rev. **D81**, 052012 (2010). arXiv:0912.5104
23. G. Aad et al. (ATLAS), Eur. Phys. J. **C75**, 229 (2015). arXiv:1412.6428
24. R. Aaij et al. (LHCb), JHEP **06**, 047 (2017). [Erratum: JHEP10,068(2017)]. arXiv:1612.07451
25. A. M. Sirunyan et al. (CMS), JHEP **02**, 032 (2018). arXiv:1712.02280
26. M. Luszczak, R. Maciula, A. Szczurek, Phys. Rev. **D85**, 094034 (2012). arXiv:1111.3255
27. A. Del Fabbro, D. Treleani, Phys. Rev. D **66**, 074012 (2002). arXiv:hep-ph/0207311
28. E.R. Cazaroto, V.P. Goncalves, F.S. Navarra, Phys. Rev. **D88**, 034005 (2013). arXiv:1306.4169
29. R. Maciula, A. Szczurek, Phys. Rev. **D96**, 074013 (2017). arXiv:1707.08366
30. E. Huayra, E.G. de Oliveira, R. Pasechnik, Eur. Phys. J. **C79**, 880 (2019). arXiv:1905.03294
31. C.F. von Weizsacker, Z. Phys. **88**, 612 (1934)
32. E.J. Williams, Phys. Rev. **45**, 729 (1934)
33. L. Frankfurt, M. Strikman, C. Weiss, Phys. Rev **D83**, 054012 (2011). arXiv:1009.2559
34. K.J. Eskola, P. Paakkinen, H. Paukkunen, C.A. Salgado, Eur. Phys. J. **C77**, 163 (2017). arXiv:1612.05741
35. R.D. Woods, D.S. Saxon, Phys. Rev. **95**, 577 (1954)
36. B. Blok, Yu. Dokshitser, L. Frankfurt, M. Strikman, Eur. Phys. J. C **72**, 1106 (1963). arXiv:2012.5533
37. B. Blok, Yu. Dokshitzer, L. Frankfurt, M. Strikman, Eur. Phys. J **C74**, 2926 (2014). arXiv:1306.3763